

ANALYSIS OF A PYROCERAM  
RADOME SUBJECTED TO  
AERODYNAMIC HEATING

JUNE 1979

APPROVED FOR PUBLIC RELEASE;  
DISTRIBUTION UNLIMITED

19990518 041

AEROSPACE STRUCTURES  
INFORMATION AND ANALYSIS CENTER

OPERATED FOR THE AIRFORCE FLIGHT DYNAMICS LABORATORY  
BY ANAMET LABORATORIES, INC.

June 26, 1979

ANALYSIS OF A PYROCERAM  
RADOME SUBJECTED TO  
AERODYNAMIC HEATING

June 1979

Approved for Public Release;  
Distribution Unlimited

*Aerospace Structures  
Information and Analysis Center*

AEROSTRUCTURES IAC  
ANAMET LABORATORIES, INC.  
100 INDUSTRIAL WAY  
SAN CARLOS, CALIFORNIA 94070  
TEL. (415) 593-2125

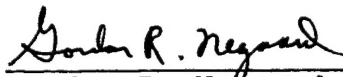
AEROSTRUCTURES IAC  
AFFDL/FBR  
WRIGHT-PATTERSON AFB,  
OHIO 45433  
TEL. (513) 255-6688

June 26, 1979

This report summarizes the analysis conducted to determine the thermal stress induced in a Pyroceram radome by aerodynamic heating. It describes the modeling and analysis of an axisymmetric radome subjected to an axisymmetric thermal distribution and the variations in the stresses produced by two different axisymmetric elements in NASTRAN. Additional analysis was conducted in which the variation was traced to the geometry of the elements. The one NASTRAN axisymmetric element supposedly capable of handling asymmetric loading cases was found to give inaccurate results as the geometry varied from a rectangular cross-section. The cyclic symmetry option in NASTRAN was investigated and appears to offer an excellent alternative for the solution of axisymmetric structures subjected to asymmetric heating such as was required in the radome analysis. This study was performed for the Air Force Materials Laboratory under ASIAC Problem No. 113.

The work was done by the Aerospace Structures Information and Analysis Center, which is operated for the Air Force Flight Dynamics Laboratory by Anamet Laboratories, under Contract No. F33615-77-C-3046.

Submitted by:



Gordon R. Negaard  
Principal Investigator

Approved by:



Conor D. Johnson, Ph.D.  
Program Manager

## TABLE OF CONTENTS

<u>Section</u>		<u>Page No.</u>
1	INTRODUCTION . . . . .	1
2	RADOME ANALYSIS . . . . .	4
3	DISC ANALYSIS . . . . .	12
4	RING ANALYSIS . . . . .	21
	REFERENCES . . . . .	30

# LIST OF ILLUSTRATIONS

<u>Figure No.</u>		<u>Page No.</u>
1	Typical Radome Configuration, Illustrating Modeling and Element Size . . . . .	5
2	Nodal Point Temperatures, °R, in Radome Nosetip . . . . .	6
3	Circumferential Stress, psi, in Radome Nosetip . . . . .	7
4	Radial Stresses, psi, in Radome Nosetip . . . . .	8
5	Axial Stresses, psi, in Radome Nosetip . . . . .	9
6	Shear Stresses, psi, in Radome Nosetip . . . . .	10
7(a)	Axisymmetric Disc Model with Rectangular Elements . . . . .	13
7(b)	Axisymmetric Disc Model with Skewed Elements . . . . .	13
8	Hoop Stress (Temperature Independent Materials) for DISC with Skewed Elements . . . . .	15
9	Radial Stress (Temperature Independent Materials) for DISC with Skewed Elements . . . . .	16
10	Axial Stress (Temperature Independent Materials) for DISC with Skewed Elements . . . . .	17
11	Hoop Stress (Temperature Dependent Materials) for DISC with Skewed Elements . . . . .	18
12	Radial Stress (Temperature Dependent Materials) for DISC with Skewed Elements . . . . .	19
13	Axial Stress (Temperature Dependent Materials) for DISC with Skewed Elements . . . . .	20
14	Axisymmetric Ring Model Subjected to Asymmetric Heating . . . . .	22
15	Hoop Stress as a Function of Angle for a Radius of .25 Inches in the Asymmetrically Heated Ring . . . . .	26

LIST OF ILLUSTRATIONS

(continued)

<u>Figure No.</u>		<u>Page No.</u>
16	Hoop Stress as a Function of Angle for a Radius of .55 Inches in the Asymmetrically Heated Ring . . . . .	27
17	Hoop Stress as a Function of Angle for a Radius of .95 Inches in the Asymmetrically Heated Ring . . . . .	28

# LIST OF TABLES

<u>Table No.</u>		<u>Page No.</u>
1	Theoretical Stress with Temperature Input for the Asymmetrically Heated Ring . . . . .	23
2	Stresses in 30° Wedge Model as a Function of Angle and Radius . . . . .	24
3	Stresses in 10° Wedge Model as a Function of Angle and Radius . . . . .	25

## SECTION 1

### INTRODUCTION

This study was conducted for the Air Force Materials Laboratory to analytically determine the aerodynamically induced thermal stresses in a radome constructed of Pyroceram 9606.

The analysis was to be conducted on ten distinct trajectories with thermal stresses calculated at three separate time steps during each trajectory. Temperature dependent material properties, the geometry of theoretical radomes, and the thermal profiles in the radomes at selected time steps in a trajectory were provided by the AFML. In order to examine many geometric and material variations as well as the thermal conditions resulting from various aerodynamic trajectories, a pre-processor was written which used the geometric and temperature output by the AFML trajectory analyses as input. This preprocessor generated a NASTRAN input deck by using the AFML nodal point temperatures for the thermal loads while using the same nodal information to generate the NASTRAN grid points and element cards. This procedure created an axisymmetric finite element model using the axisymmetric elements in NASTRAN, primarily the trapezoidal CTRAPRG and CTRAPAX elements, although some use was made of the triangular CTIRARG and CTIRIAX elements.

The initial analyses consisted of radomes subjected to axisymmetric aerodynamic heating, with the highest temperature gradients occurring about eight seconds after launch. Models using both the CTRAPAX and the CTRAPRG elements were analyzed at six, eight and ten seconds after launch. These results showed high stresses at the radome nosetip. Evaluation of the thermal fields showed higher temperature gradients in the axial direction than in the thickness direction of the radome due to the geometry of the elements. A finer AFML model was therefore generated which would cut the axial gradient to about 300°F instead of the 600°F which existed in the first model. This



reduced the stresses some, but they still appeared to be too high, so a further iteration was made reducing the maximum temperature between any two elements to approximately 200°F. This was about as fine as the AFML thermal model could go since it was limited to around 380 nodes. In addition, the aspect ratios in the area of interest had been reduced to approximately one-to-one. For this model, the CTRAPRG solution predicted maximum compressive thermal stresses of about 21000 psi, which agreed well with a SAAS III analysis performed by the AFML. The CTRAPAX elements, however, predicted stresses as much as 100% higher.

The reason for the variation in the stresses predicted by the two elements was unknown. According to theory, the stresses should have been identical for axisymmetric loading. Various ways of modeling the radome with triangular elements were also investigated to determine if the problem was a function of modeling techniques. This did not appear to be so since all combinations of AX elements produced essentially similar answers, and the RG elements likewise produced a set of similar stresses. It was necessary to pursue this discrepancy further since the AFML requested ASIAC to investigate thermal stresses due to non-axisymmetric aerodynamic heating instead of continuing the symmetrically loaded thermal cases. Since only the CTRAPAX and CTRIAAX elements could handle asymmetric loading, it was necessary to determine the reliability of these elements. For this purpose, a simple disc model with known theoretical solutions was examined [1]\*. A quadratically varying radial temperature and a linearly varying axial temperature were examined to see if the discrepancy was due to the two-dimensional nature of the thermal field being applied. For temperature independent material properties, CTRAPRG and CTRAPAX models agreed exactly with the theoretical solution as long as all

---

\*Numbers in brackets indicate references at end of report.

elements were rectangularly shaped. When the shapes were changed to a non-rectangular parallelogram, the CTRAPAX predicted radial stresses 60 to 80 percent higher than the theoretical, while the CTRAPRG stresses remained exact. Similar runs with temperature dependent material properties produced similar results. Even worse, the CTRAPAX model predicted axial stresses as high as 27000 psi, when the theoretical solution and the CTRAPRG results predicted no axial stress. This effect was shown to be essentially aspect ratio independent, depending almost entirely on the degree of skewness of the parallelograms.

Since it was very difficult to model the radomes without using skewed triangles or parallelograms, a different approach was needed. The cyclic symmetry option in NASTRAN was examined. A ring model was constructed using the solid CIHEXI elements with four elements in the axial direction, eight in the radial direction, and one in the circumferential direction, forming a thirty degree wedge. Theoretical solutions exist for a ring subjected to a temperature distribution of the form  $T_0 r^k \cos n\theta$ , where  $k$  and  $n$  are integers [2]. The NASTRAN results were compared to the theoretical predictions for both rectangular shaped and skewed parallelepiped elements. These produced almost identical stresses so this technique does not appear to be sensitive to the geometry used for the elements. The stresses were about ten percent lower than theoretical, but this can be attributed to the large arc used to model the wedge. Reducing the wedge to ten degrees produced much better results, but the computer time required increased proportionately.

When compared to the axisymmetric elements, the cyclic symmetry option appears to offer an excellent alternative for the solution of axisymmetric structures subjected to asymmetric heating such as required in this type of radome analysis.

## SECTION 2

### RADOME ANALYSIS

The basic radome shape used in the analysis is shown in Figure 1. The plot is approximately actual size, except that it is shortened by omitting most of the center section. The actual model simulated was an ogive 19.6 inches long, 6.5 inches in diameter at the base and .281 inches thick. This model contained 9 nodes through the thickness and 40 in the axial direction, with a total of 339 grid points and 296 CTRAPRG and CTRIARG elements. The spacing of the nodal points was dictated by the AFML program which calculated the temperature distribution as a function of the trajectory. This program output temperature at the centers of seven elements through the thickness, plus the temperature at the inner and outer surface of the shell. These points were then used as NASTRAN grid points with the corresponding nodal point temperatures.

The aerodynamic heating created high temperature gradients in both the axial and radial direction. Because of the temperature dependent material properties, it was desirable to keep these gradients as small as possible. Figure 2 represents the best distribution of thermal gradients that was obtainable at the nosetip. This distribution produced the circumferential, radial, axial, and shear stresses shown in Figures 3 through 6. These figures also show the element selection that produced the most consistent set of stresses. Comparison with Figure 2, which was the original element orientation, shows that the triangular elements have been moved to the inner surface of the model instead of being at the outer surface. It can be observed that the stresses in the triangles do not appear consistent with the stresses in the neighboring trapezoidal elements. Several other types of modeling were tried, including all triangular elements; however, the triangular elements always appeared to produce stress fields with sudden changes or stress reversals.

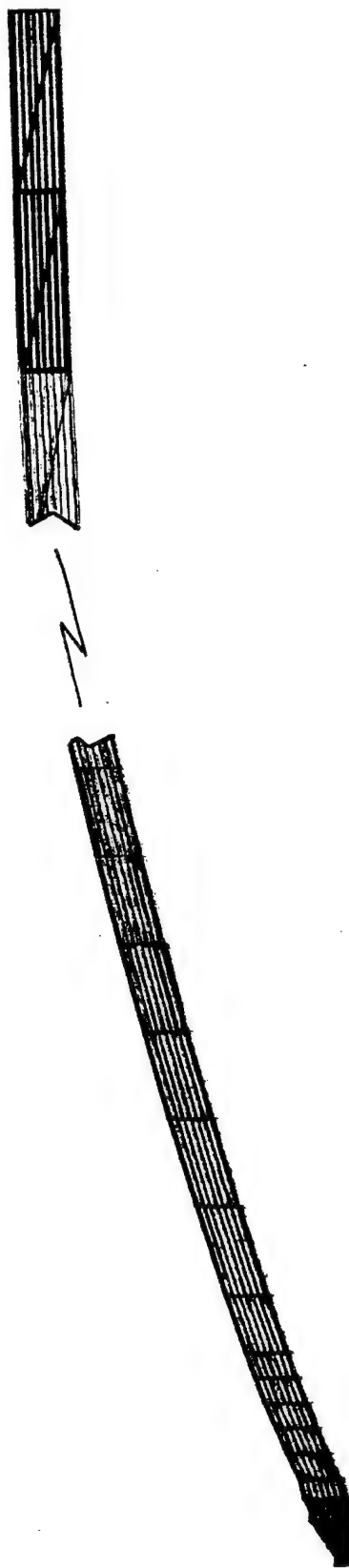


Figure 1. Typical Radome Configuration, Illustrating Modeling and Element Size

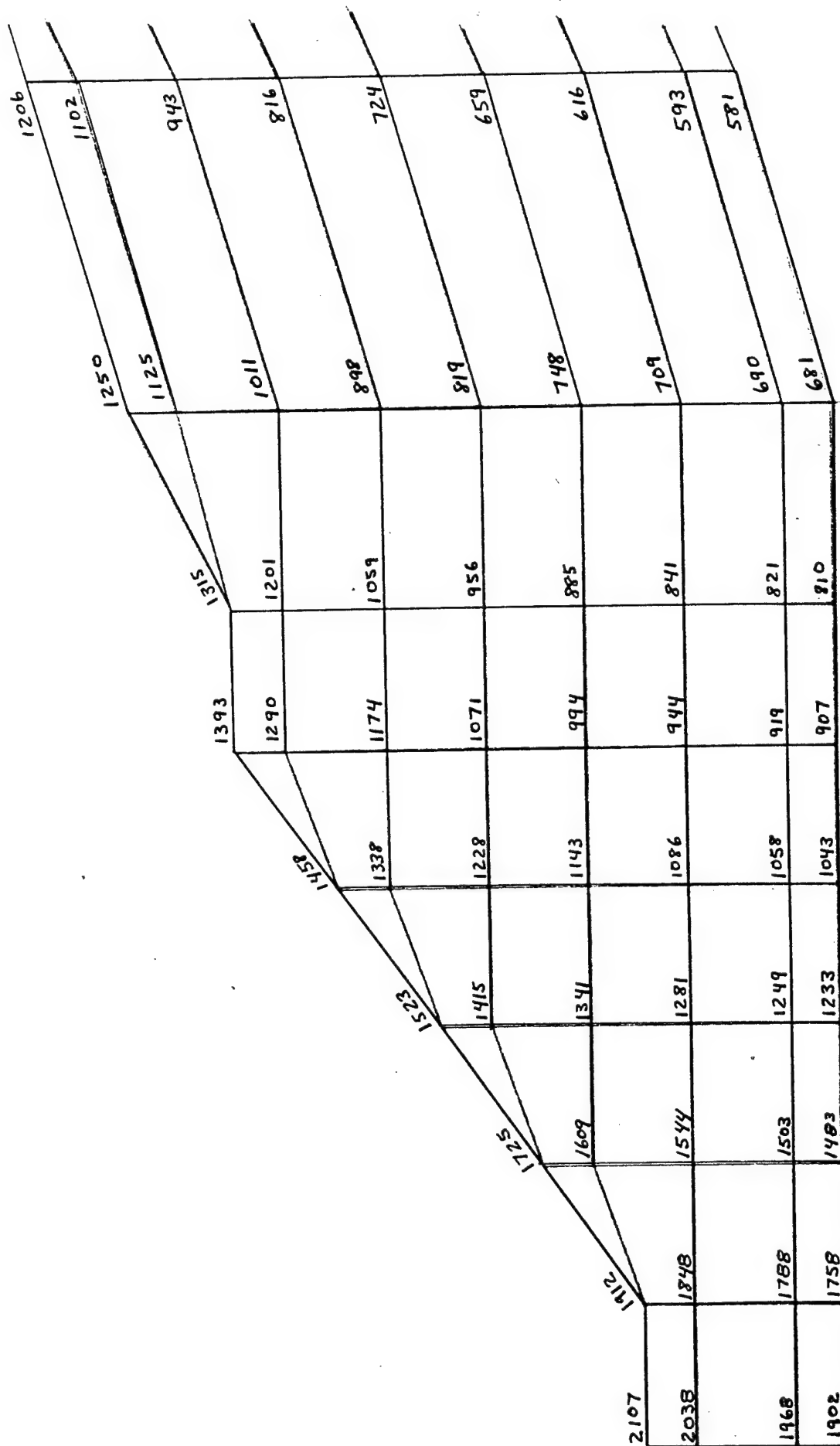


Figure 2. Nodal Point Temperatures, °R, in Radome Nostip



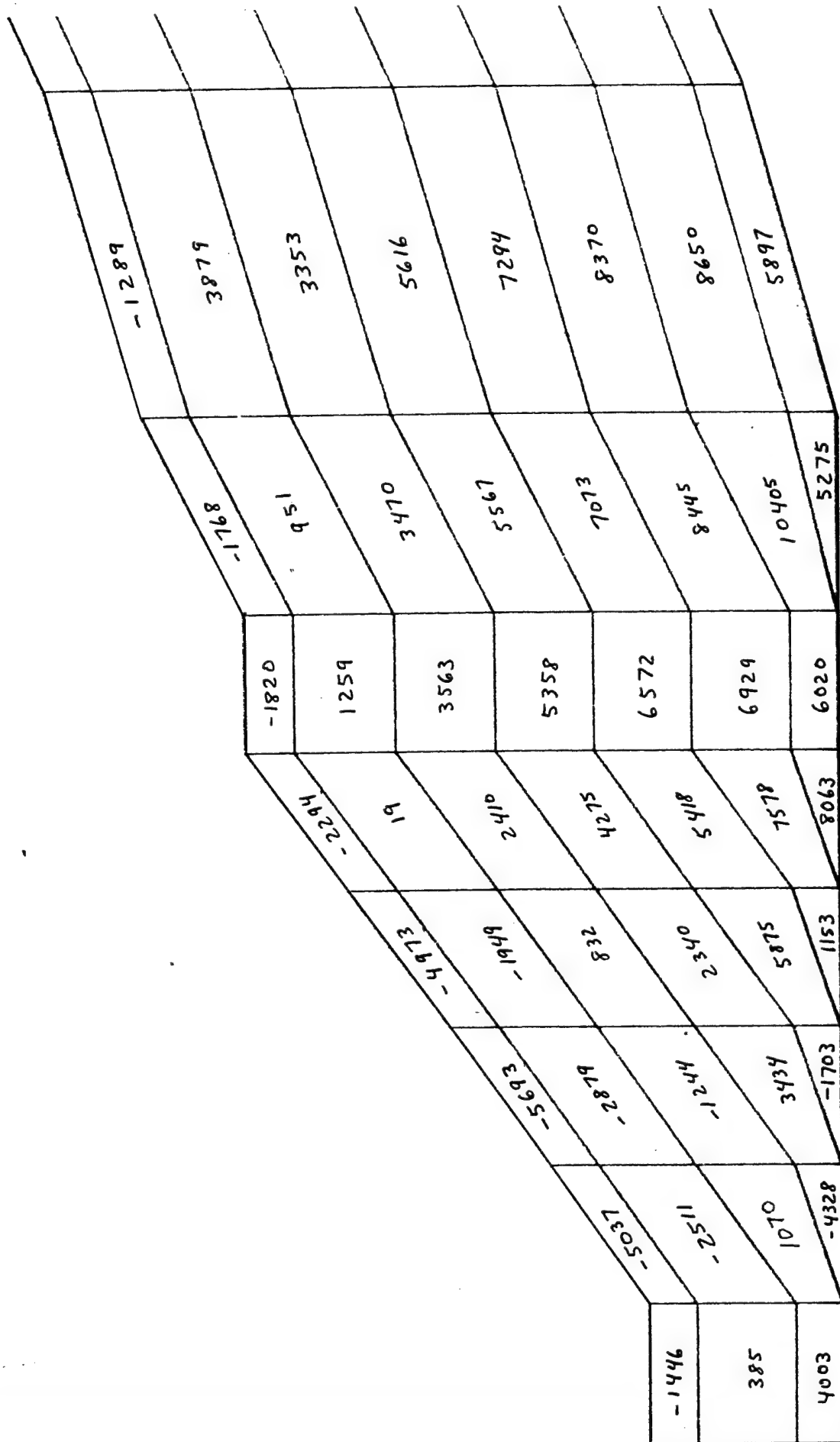


Figure 4. Radial Stresses, psi, in Radome Nosetip

-1000	-7067	9264	-11344	-11354	-15958	-18653	-19334
1205	1185	9488	10190	12494	13612	16333	15944
-828	6676	11069	14016	16207	13847	19032	14325
	5258	10962	15352	25427	7954	23813	
					9170	8423	12252
					2565	1392	6886
					-6171	-8082	-836
					-15958	-18653	-19334

Figure 5. Axial Stresses, psi, in Radome Nostetip



-696	-5387	8361	-8384	3333	-5447	-1562	-49
-116	2394	4815	5416	5253	-5367	5202	-4990
2065	2471	3103	3423	3115	-4168	-3179	-2766
	8007	8551	8111	1319	-2621	-1841	-978
		1754	1024	682	-1436	-838	304
					-449	160	1336
					4916	3798	2233
						2132	5248

Figure 6. Shear Stresses, psi, in Radome Nostip

CTRAPAX and CTRIAAX elements were also examined, but these elements exhibited stresses as high as 30,000 to 40,000 psi for the same temperature distributions.

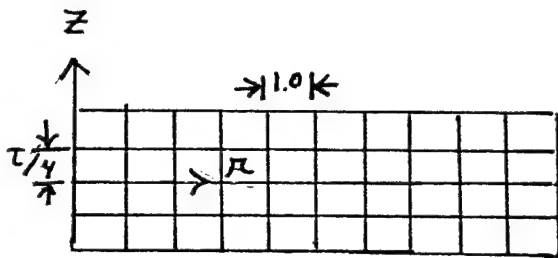
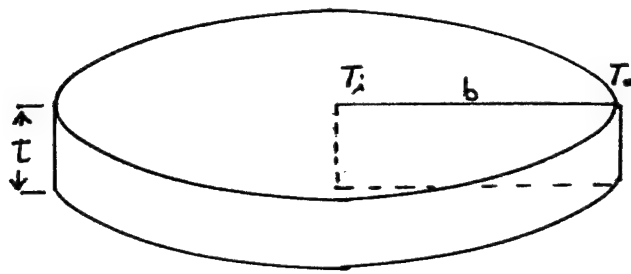
The AFML accepted the results as shown in Figures 3, 4, 5 and 6 as being consistent with stresses calculated by SAAS III, and thus, decided that SAAS III could be used to complete the analysis of the axisymmetric heating. Based on the stress levels shown by this analysis, AFML decided that the nosetip would be removed from the new model and replaced by a steel plug to relieve the thermal stresses. These results and the decision to insert a metal nosetip parallels closely a similar analysis of a silicon nitride radome subjected to aerodynamic heating using SAAS II [3].

### SECTION 3

#### DISC ANALYSIS

In order to determine why the CTRAPAX and CTRAPRG elements produced differing results for the radome model, a simple disc model restrained at the outer circumference which had known theoretical solutions was chosen [1]. Both a quadratically varying radial temperature and a linearly varying axial temperature could be applied. This model and a cross-section of the axisymmetric model is shown in Figure 7(a). For this model, both types of elements produced exact theoretical answers for aspect ratios varying from 1.0 to 10.0 for temperature independent material properties for combinations of radially and axially varying temperatures. This eliminated aspect ratios and two-dimensional temperature gradients as being responsible for the differing results in the radome. There was no theoretical solution for temperature dependent material properties; however, both elements still produced identical answers. This also eliminated temperature dependent properties as being the cause, leaving geometry of the elements as the only likely remaining candidate.

The geometry of the elements was changed, as shown in Figure 7(b), so that all elements had at least one skewed side instead of being rectangular. This model was then run with only the radially varying temperature distribution. These runs produced results that definitely proved that the CTRAPAX elements produced incorrect results when a non-rectangular cross-section is used. For the temperature independent results, the CTRAPRG elements produced results which matched the theoretical solution exactly, while the CTRAPAX elements gave radial and hoop stresses sixty to one hundred percent too high. Even worse, these elements predicted axial stresses almost as high as the axial and radial stresses, while the CTRAPRG results agreed with the theoretical solution of zero stress. The



$$T(r) = T_o + (T_i - T_o) \left[ 1 - \frac{r^2}{b^2} \right]$$

$$\sigma_r(r) = -\frac{1}{4} E \alpha (T_i - T_o) \left[ \frac{3-\nu}{1-\nu} - \frac{r^2}{b^2} \right]$$

$$\sigma_\theta(r) = -\frac{1}{4} E \alpha (T_i - T_o) \left[ \frac{3-\nu}{1-\nu} - \frac{3r^2}{b^2} \right]$$

$$\sigma_z(r) = 0$$

$$b = 10'' \quad T_i = 1200^\circ R$$

$$E = 10^7 \text{ psi} \quad T_o = 200^\circ R$$

$$\alpha = 10^{-6} \text{ in/in/}^\circ R$$

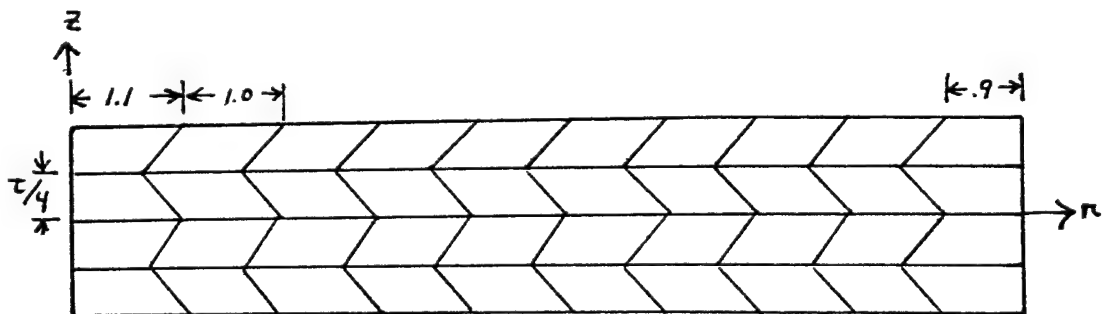
$$\nu = 1/3$$

$$T(r) = 1200 - 10r^2$$

$$\sigma_r(r) = -25(400 - r^2)$$

$$\sigma_\theta(r) = -25(400 - 3r^2)$$

Figure 7(a). Axisymmetric Disc Model with Rectangular Elements



Elements Changed To Parallelograms  
Centroids of Elements Remained Unchanged in Radial Direction

Figure 7(b). Axisymmetric Disc Model with Skewed Elements

temperature dependent material runs predicted stresses that followed the same pattern but, of course, could not be compared to the theoretical solution. These results are shown in Figures 8 through 13.

This analysis showed that the CTRAPRG elements appeared to produce reliable results while confirming that the CTRAPAX elements could not be trusted in a model requiring the use of non-rectangular element shapes. This essentially ruled out the use of the CTRAPAX elements in a model simulating a radome shape. Since only the CTRAPAX and CTRIAAX elements can be used for axisymmetric models subjected to non-axisymmetric loads, it was necessary to look for an alternate way of solving the asymmetric aerodynamic heating problem.

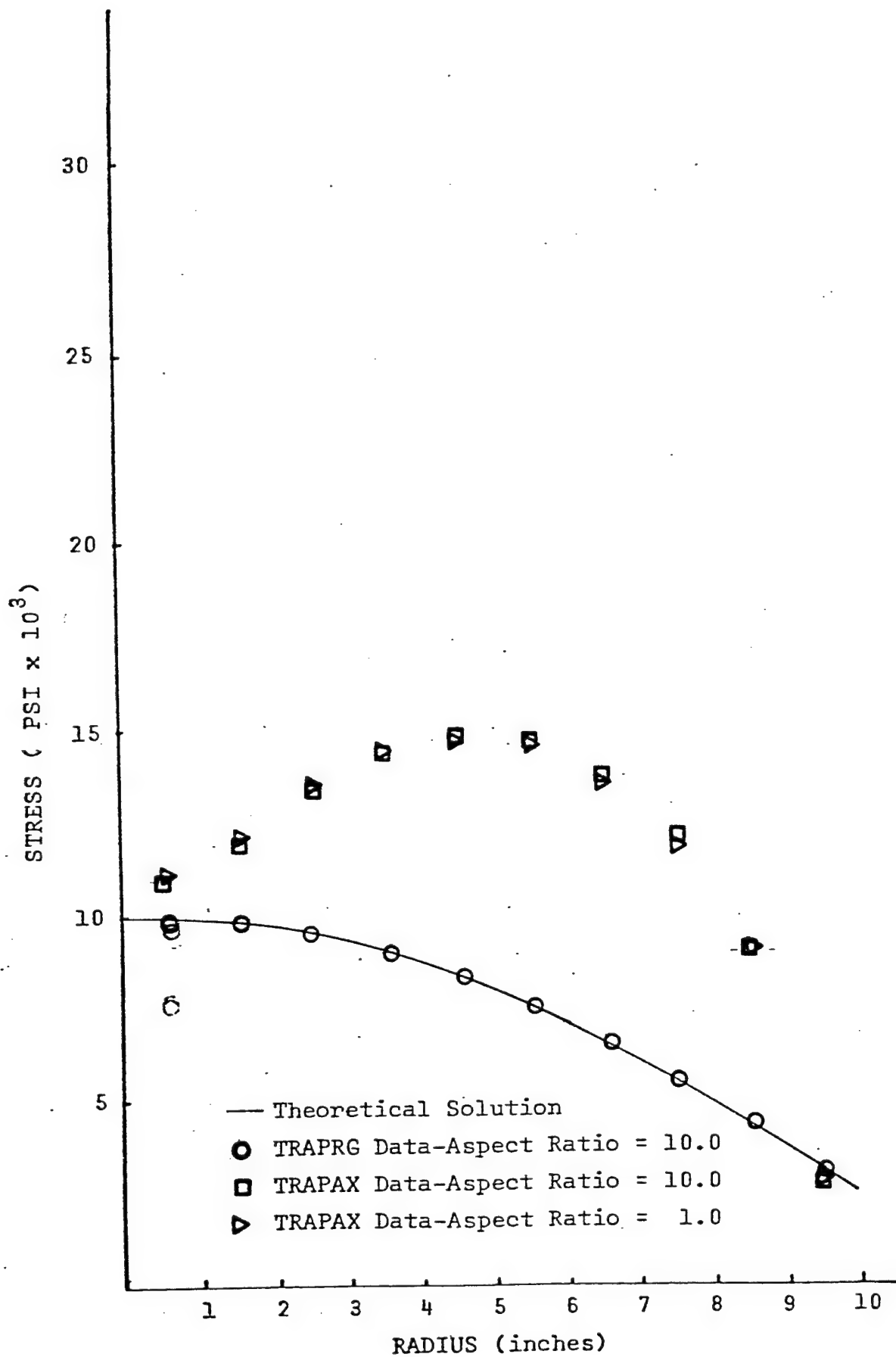


Figure 8. Hoop Stress (Temperature Independent Materials) for DISC with Skewed Elements

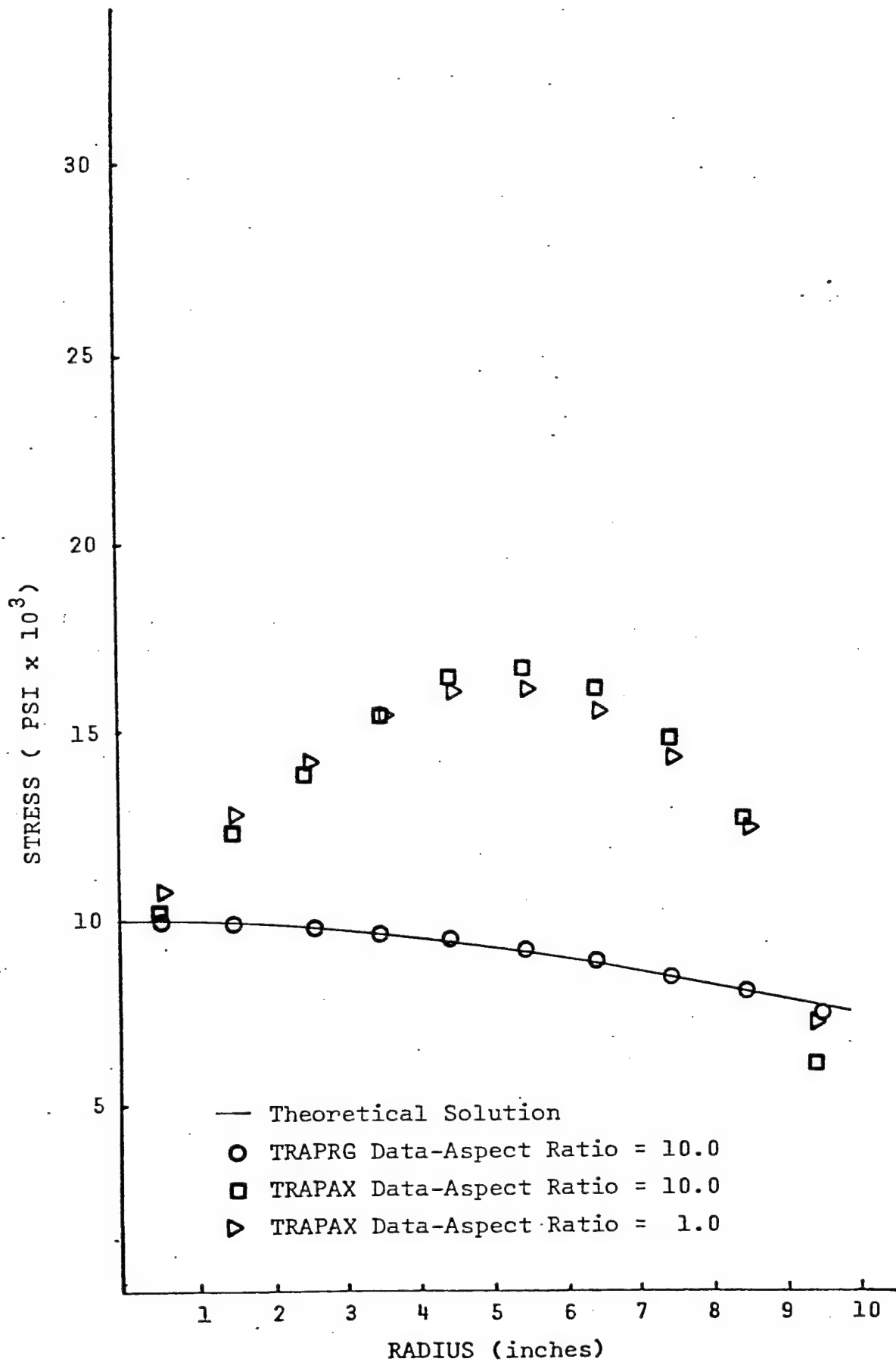


Figure 9. Radial Stress (Temperature Independent Materials) for DISC with Skewed Elements

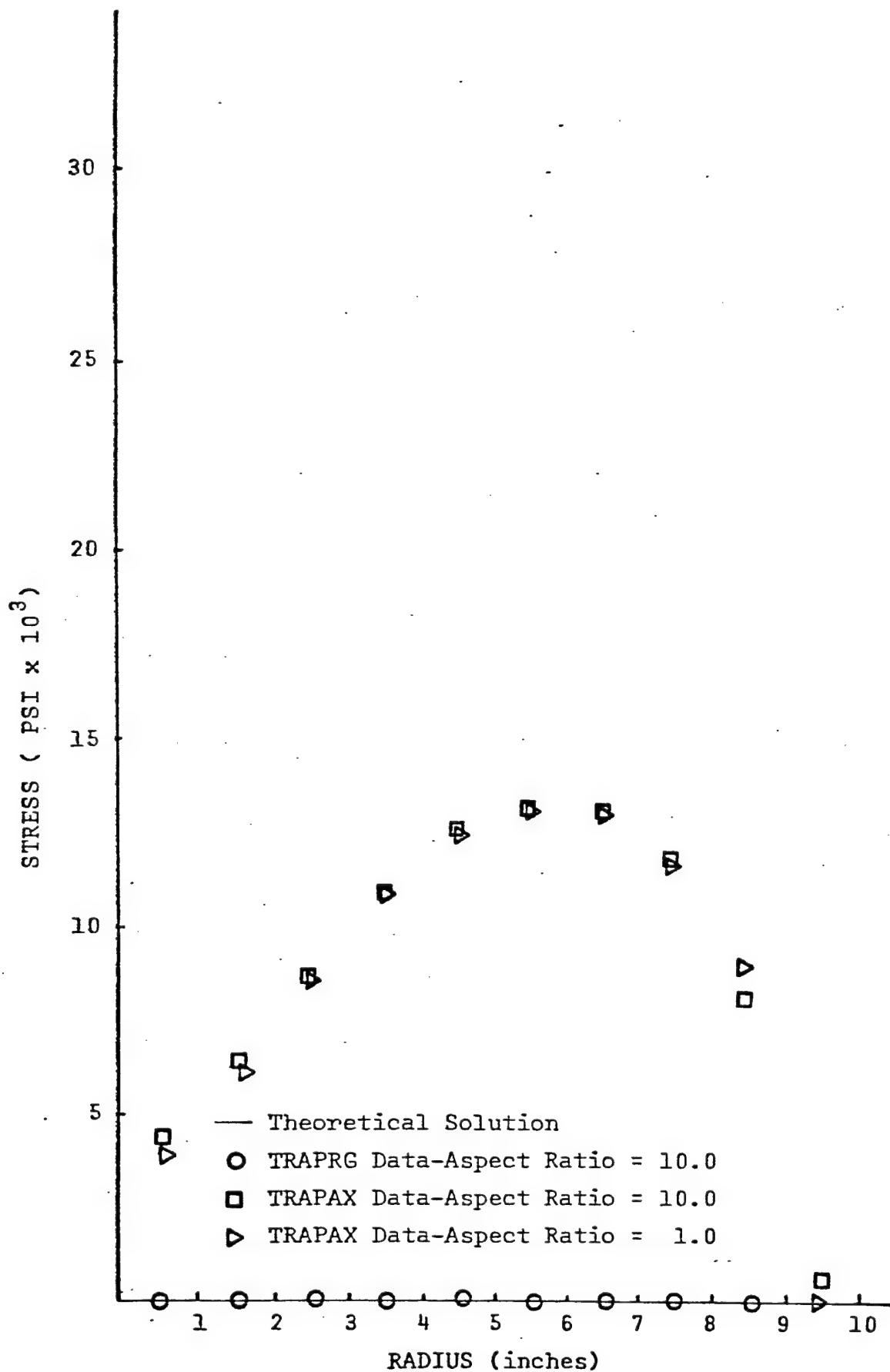


Figure 10. Axial Stress (Temperature Independent Materials) for DISC with Skewed Elements



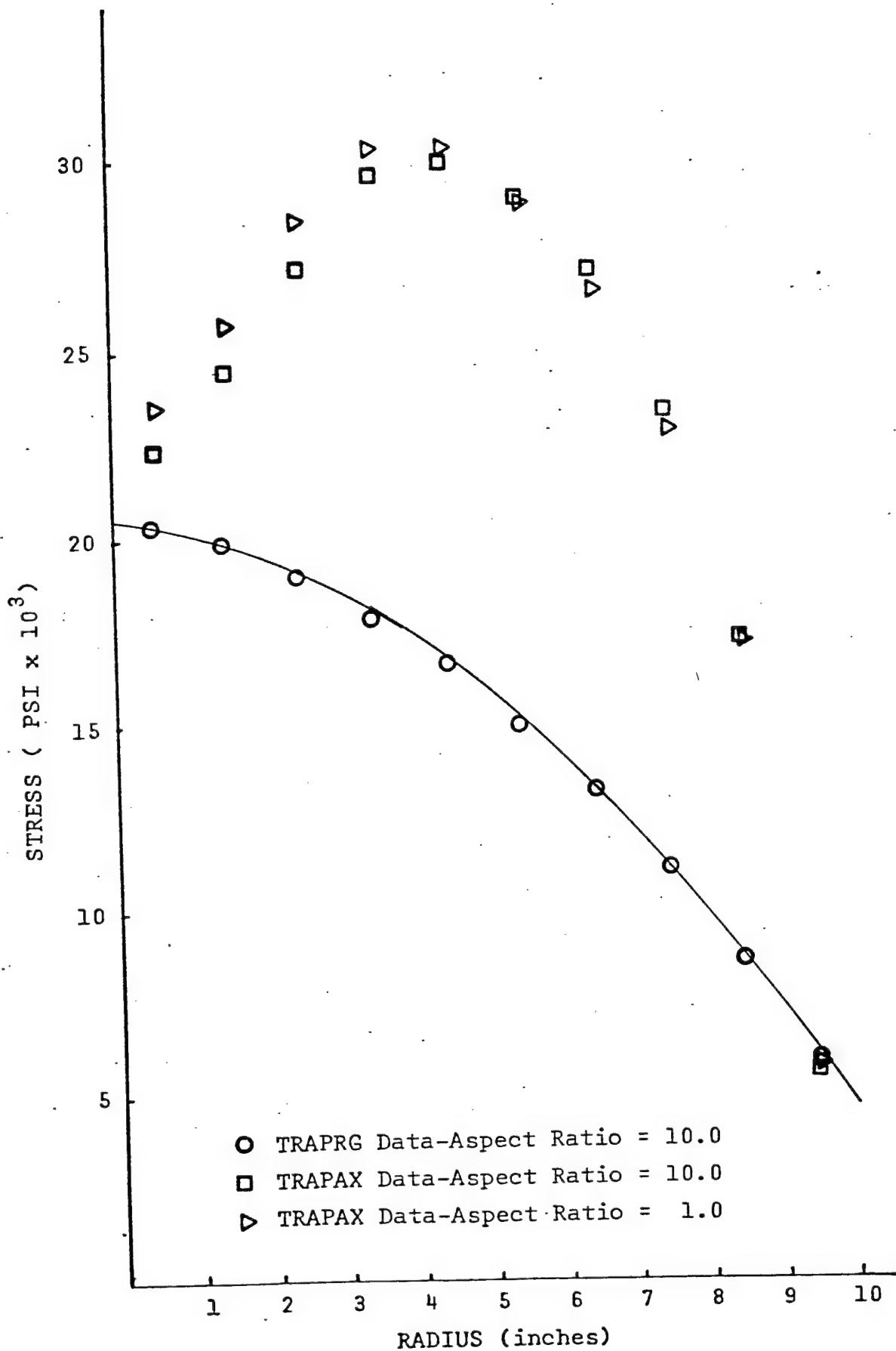


Figure 11. Hoop Stress (Temperature Dependent Materials) for DISC with Skewed Elements

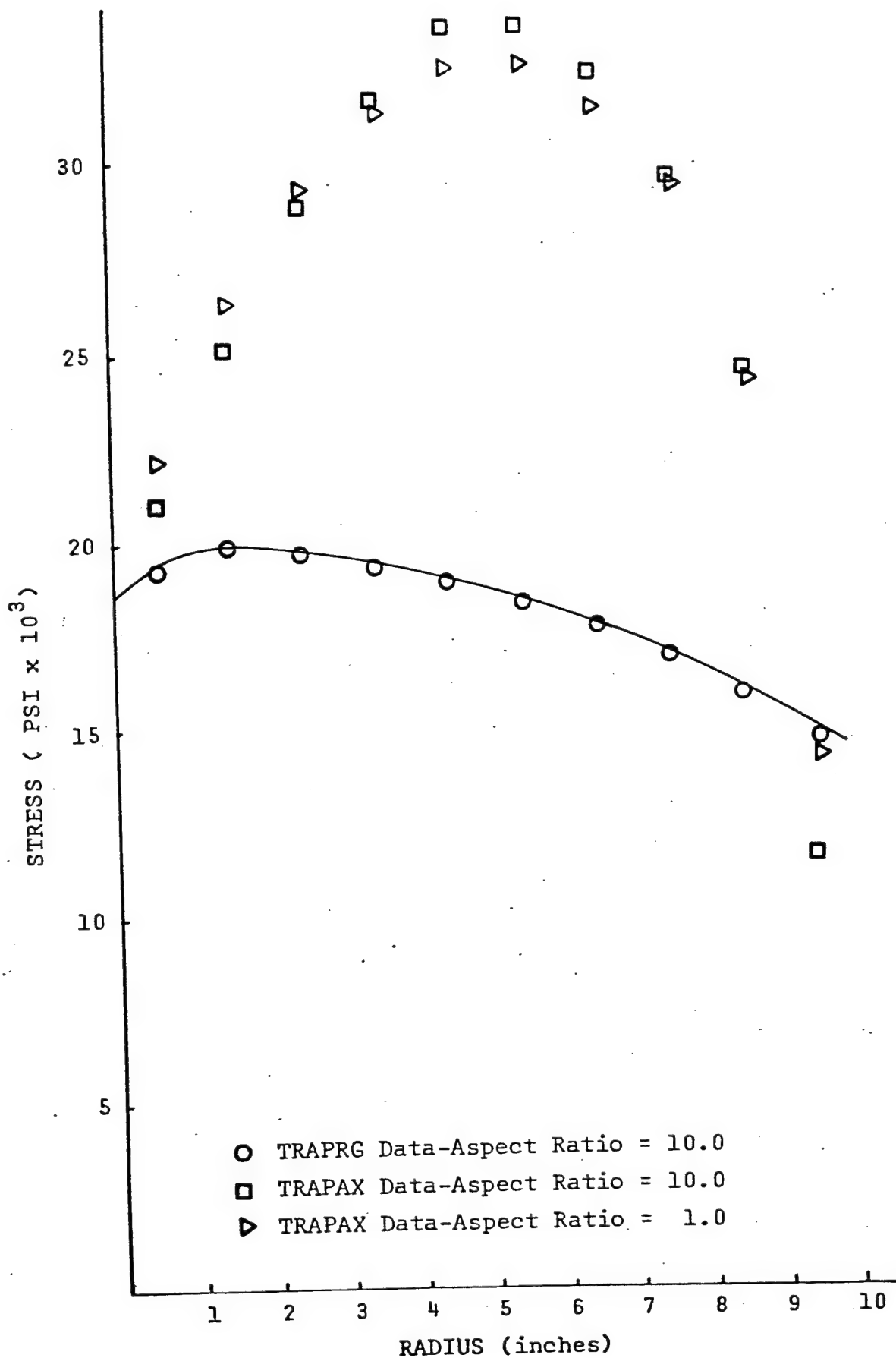


Figure 12. Radial Stress (Temperature Dependent Materials) for DISC with Skewed Elements

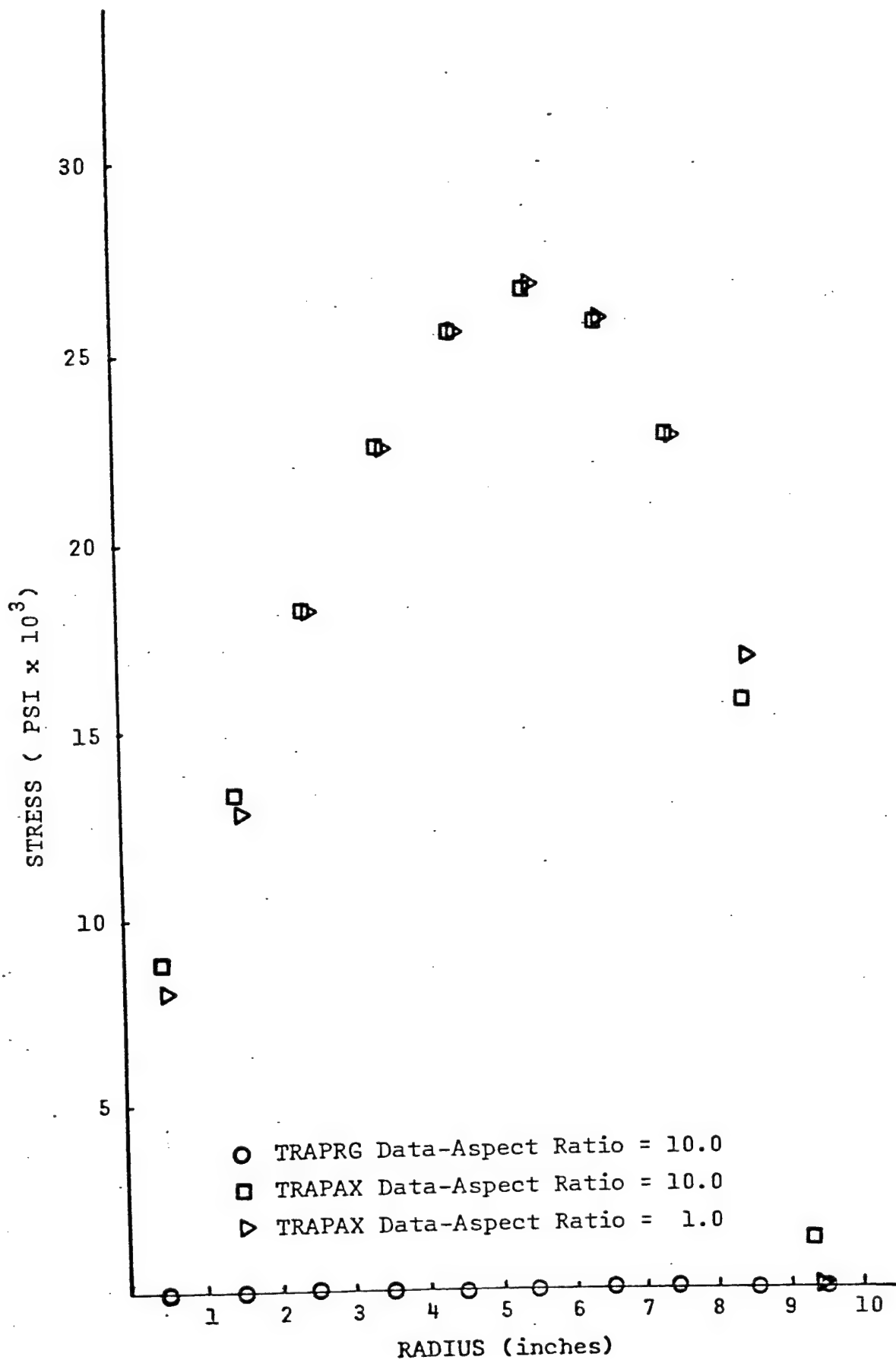


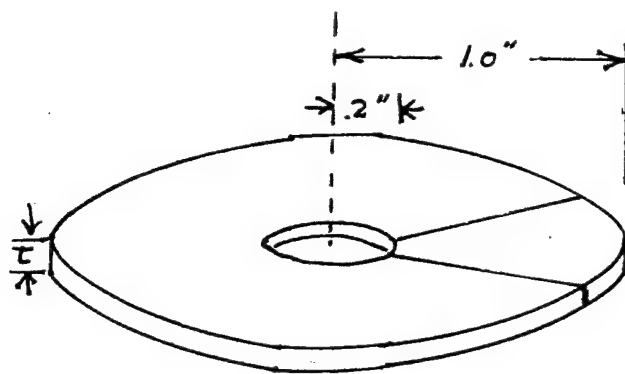
Figure 13. Axial Stress (Temperature Dependent Materials) for DISC with Skewed Elements

## SECTION 4

### RING ANALYSIS

The cyclic symmetry option in NASTRAN was examined to determine if better results for symmetric structures subjected to an asymmetric thermal load could be obtained. A ring subjected to a temperature distribution of the form  $T = T_0 r^k \cos n\theta$  was chosen because theoretical solutions could be obtained [2]. The model of the ring is shown in Figure 14. Both thirty degree and ten degree wedge shapes were examined, requiring twelve and thirty-six load cases, respectively, when running cyclic symmetry. The model cross section was deliberately made as similar to the previous disc analysis as possible, including the use of skewed elements shapes. Table 1 shows the temperatures used as input and the resulting theoretical hoop and radial stresses. The axial stress should be identically zero. The actual stresses obtained at several radii are shown in Tables 2 and 3 for both ten and thirty degree wedges with skewed and non-skewed geometry. It can be seen that skewness had little effect except for the radial stress in the outermost elements. The axial stresses tended to be less than ten percent of the lower of the radial or hoop stress, except at the outer fiber. It was discovered that the axial stresses could be made smaller by making the ring thinner; thus, approaching a state of plane stress more closely. Selected plots of hoop stress are shown as Figures 15, 16 and 17. It can be seen in these figures that as the wedge becomes narrower, it appears to approach the theoretical solution as a limit.

In order to make a comparison of the computer costs of cyclic symmetry against the use of the axisymmetric elements, a ring model with the same geometry using the CTRAPAX elements with non-skewed geometry and temperature input at every fifteen degrees, as shown in Table 1, was examined. This produced almost exact theoretical answers; however, the axisymmetric model

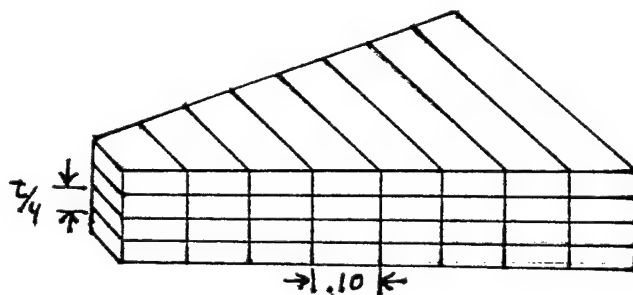


$$T = T_o \left\{ \frac{r}{b} \right\}^2 \cos \theta$$

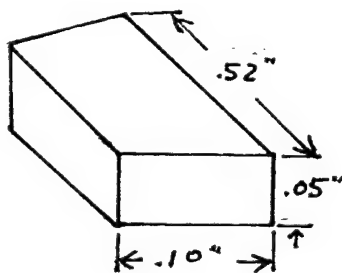
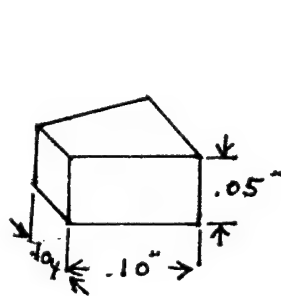
$$\sigma_{rr} = E \alpha T_o B_k \cos \theta$$

$$\sigma_{\theta\theta} = E \alpha T_o D_k \cos \theta$$

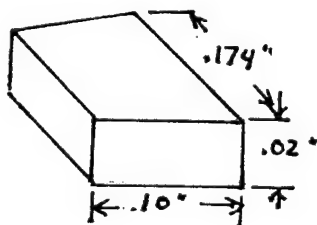
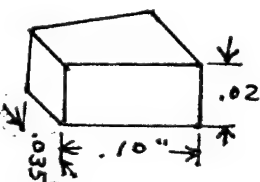
$r$	$B_k$	$D_k$
.2	0.0	.1202
.3	.03258	.1177
.4	.04408	.1163
.5	.04808	.1024
.6	.04696	.07364
.7	.04144	.02929
.8	.03170	-.03088
.9	.01788	-.1070
1.0	0.0	-.1990



CIHEX WEDGE MODEL USED FOR CYCLIC SYMMETRY



30° WEDGE ASPECT  
RATIO RANGE  
2/1 to 10/1



10° WEDGE ASPECT  
RATIO RANGE  
5/1 to 9/1

Figure 14. Axisymmetric Ring Model Subjected to Asymmetric Heating

Table 1. THEORETICAL STRESS WITH TEMPERATURE INPUT  
FOR THE ASYMMETRICALLY HEATED RING

TEMPERATURES AS A FUNCTION OF R-SQUARED AND COSINE THETA										
THETA (DEGREES)	R=	.2	.3	.4	.5	.6	.7	.8	.9	1.0
0.00		8.00	10.00	12.00	14.00	16.00	18.00	20.00	22.00	24.00
15.00		7.73	17.39	30.91	48.30	69.55	94.06	123.64	158.48	193.19
30.00		6.93	15.59	27.71	43.30	62.30	84.37	110.85	140.30	173.21
45.00		5.65	12.73	22.63	35.36	50.91	69.30	90.51	114.56	141.43
60.00		4.06	9.00	16.00	25.00	36.00	49.01	64.01	81.01	100.01
75.00		2.07	4.66	8.29	12.93	18.64	25.37	33.14	41.94	51.78
90.00		.00	.00	.00	.01	.01	.01	.01	.02	.02
105.00		-2.07	-4.66	-8.28	-12.93	-18.63	-25.35	-33.11	-41.91	-51.74
120.00		-4.06	-9.00	-16.00	-24.93	-35.99	-48.99	-63.98	-80.97	-99.97
135.00		-5.65	-12.73	-22.62	-35.35	-50.90	-69.28	-90.49	-114.53	-141.40
150.00		-6.93	-15.59	-27.71	-43.30	-62.30	-84.36	-110.84	-140.26	-173.19
165.00		-7.73	-17.39	-30.91	-48.29	-69.54	-94.06	-123.63	-158.47	-193.17
180.00		-8.00	-18.00	-32.00	-50.00	-72.00	-96.00	-128.00	-162.00	-200.00

HOOP STRESS AS A FUNCTION OF R-SQUARED AND COSINE THETA										
THETA (DEGREES)	R=	.2	.3	.4	.5	.6	.7	.8	.9	1.0
0.00		240.45	235.40	232.00	226.85	147.25	55.58	-21.76	-214.50	-395.00
15.00		232.21	227.33	224.63	197.62	142.26	56.58	-59.66	-206.71	-384.44
30.00		218.20	203.87	201.44	177.37	127.95	31.73	-53.49	-135.53	-344.59
45.00		179.00	166.46	164.48	144.82	104.15	41.42	-43.67	-151.53	-261.44
60.00		122.22	117.72	116.52	102.41	75.05	29.29	-32.86	-127.01	-195.03
75.00		62.24	60.95	60.22	53.93	36.13	15.17	-15.99	-55.41	-115.05
90.00		0.00	0.00	0.00	0.00	0.00	0.00	0.00	0.00	0.00
105.00		-62.19	-60.90	-60.17	-52.93	-36.10	-15.15	15.98	55.36	102.96
120.00		-120.17	-117.67	-116.27	-102.37	-75.62	-29.28	31.27	106.97	195.95
135.00		-169.95	-166.42	-164.44	-144.73	-104.12	-41.42	43.66	151.29	261.38
150.00		-208.17	-203.64	-201.42	-177.34	-127.93	-50.73	53.46	135.51	344.64
165.00		-232.20	-227.37	-224.66	-197.81	-142.25	-50.58	59.65	206.70	384.42
180.00		-240.45	-235.40	-232.00	-204.85	-147.25	-55.58	21.76	214.50	395.00

RADIAL STRESSES AS A FUNCTION OF R-SQUARED AND COSINE THETA										
THETA (DEGREES)	R=	.2	.3	.4	.5	.6	.7	.8	.9	1.0
0.00	0.00	62.94	85.16	96.15	98.92	82.03	53.40	35.76	0.00	0.00
15.00	0.00	62.94	85.16	96.15	98.92	82.03	53.40	35.76	0.00	0.00
30.00	0.00	56.43	76.35	83.23	81.34	71.75	54.91	38.97	0.00	0.00
45.00	0.00	46.08	62.34	68.00	66.42	56.01	44.83	25.29	0.00	0.00
60.00	0.00	32.53	44.09	48.09	46.97	41.45	31.70	17.86	0.00	0.00
75.00	0.00	16.87	22.83	24.90	24.32	21.46	16.42	9.26	0.00	0.00
90.00	0.00	.01	.01	.01	.01	.01	.01	.00	0.00	0.00
105.00	0.00	-16.86	-22.81	-24.85	-24.30	-21.44	-16.40	-9.25	0.00	0.00
120.00	0.00	-32.57	-44.07	-48.07	-46.95	-41.43	-31.69	-17.68	0.00	0.00
135.00	0.00	-46.07	-62.33	-67.95	-66.40	-56.05	-44.82	-25.20	0.00	0.00
150.00	0.00	-56.42	-76.34	-83.27	-81.33	-71.77	-54.91	-38.97	0.00	0.00
165.00	0.00	-62.94	-85.15	-92.03	-90.71	-80.05	-61.24	-34.54	0.00	0.00
180.00	0.00	-62.94	-85.16	-96.15	-98.92	-82.03	-53.40	-35.76	0.00	0.00

Table 2. STRESSES IN 30° WEDGE MODEL AS A  
FUNCTION OF ANGLE AND RADIUS

THETA (Degrees)	Ring With <u>Unskewed Elements</u>			Ring With <u>Skewed Elements</u>		
	<u>RADIAL</u>	<u>HOOP</u>	<u>AXIAL</u>	<u>RADIAL</u>	<u>HOOP</u>	<u>AXIAL</u>
STRESSES AT .25 INCH RADIUS						
0	41	187	-4	42	187	-3
30.0	35	162	-4	36	162	-2
60.0	20	93	-2	21	94	-2
90.0	0	0	0	0	0	0
STRESSES AT .55 INCH RADIUS						
0	87	158	8	87	158	9
30.0	76	137	7	76	137	8
60.0	43	79	4	44	79	5
90.0	0	0	0	0	0	0
STRESSES AT .95 INCH RADIUS						
0	26	-221	43	26	-221	43
30.0	23	-192	37	22	-192	37
60.0	13	-111	22	13	-111	21
90.0	0	0	0	0	0	0

Table 3. STRESSES IN 10° WEDGE MODEL AS A  
FUNCTION OF ANGLE AND RADIUS

THETA (Degrees)	Ring With <u>Unskewed Elements</u>			Ring With <u>Skewed Elements</u>		
	<u>RADIAL</u>	<u>HOOP</u>	<u>AXIAL</u>	<u>RADIAL</u>	<u>HOOP</u>	<u>AXIAL</u>
STRESSES AT .25 INCH RADIUS						
0.0	46	224	-8	50	224	-5
30.0	40	194	-7	43	194	-5
60.0	23	112	-4	25	112	-3
90.0	0	0	0	0	0	0
STRESSES AT .55 INCH RADIUS						
0.0	101	178	0	102	180	2
30.0	87	154	0	89	156	1
60.0	50	89	0	51	90	1
90.0	0	0	0	0	0	0
STRESSES AT .95 INCH RADIUS						
0.0	28	-276	33	18	-279	33
30.0	25	-239	28	16	-242	29
60.0	14	-138	16	9	-140	17
90.0	0	0	0	0	0	0



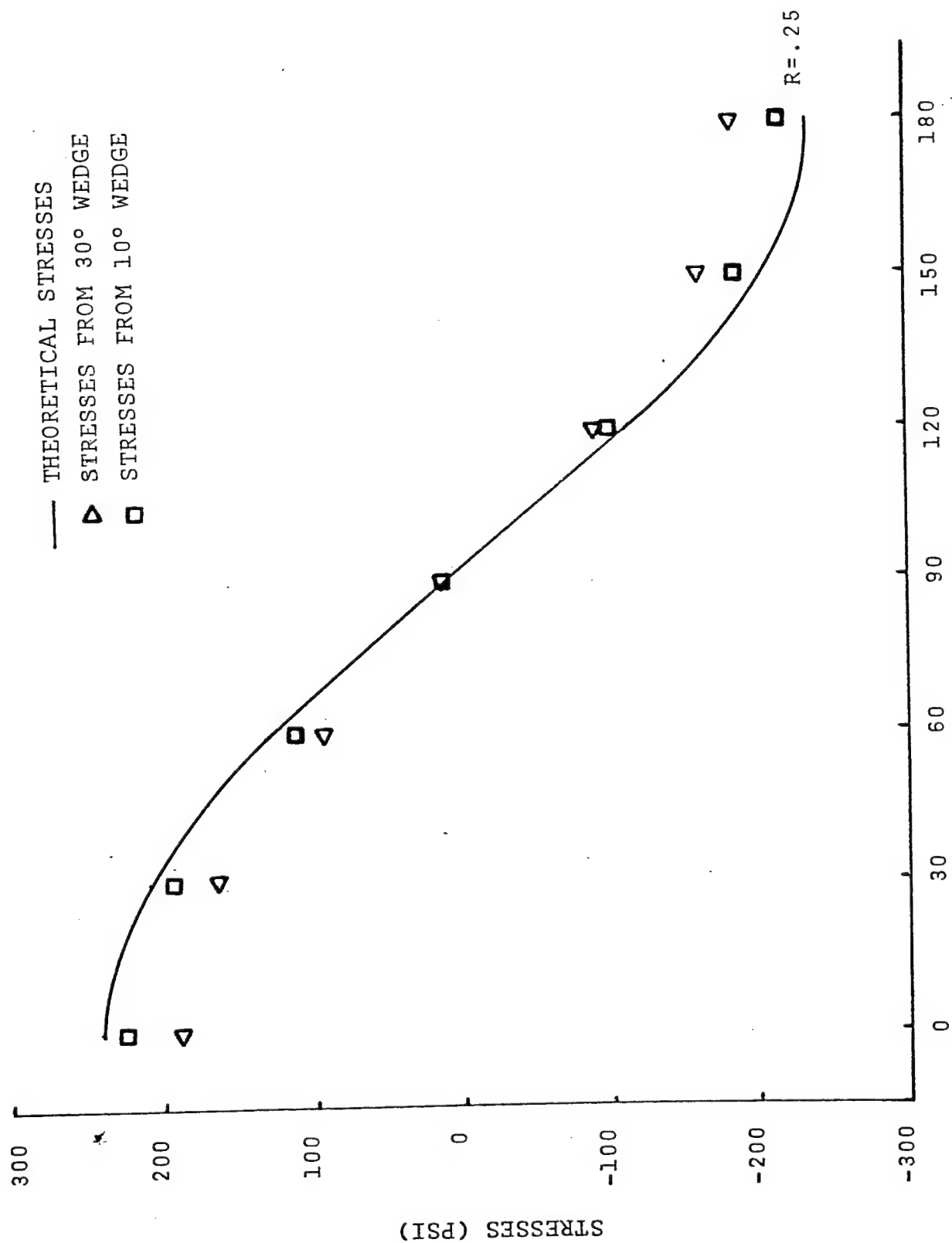


Figure 15. Hoop Stress as a Function of Angle for a Radius of .25 Inches in the Asymmetrically Heated Ring

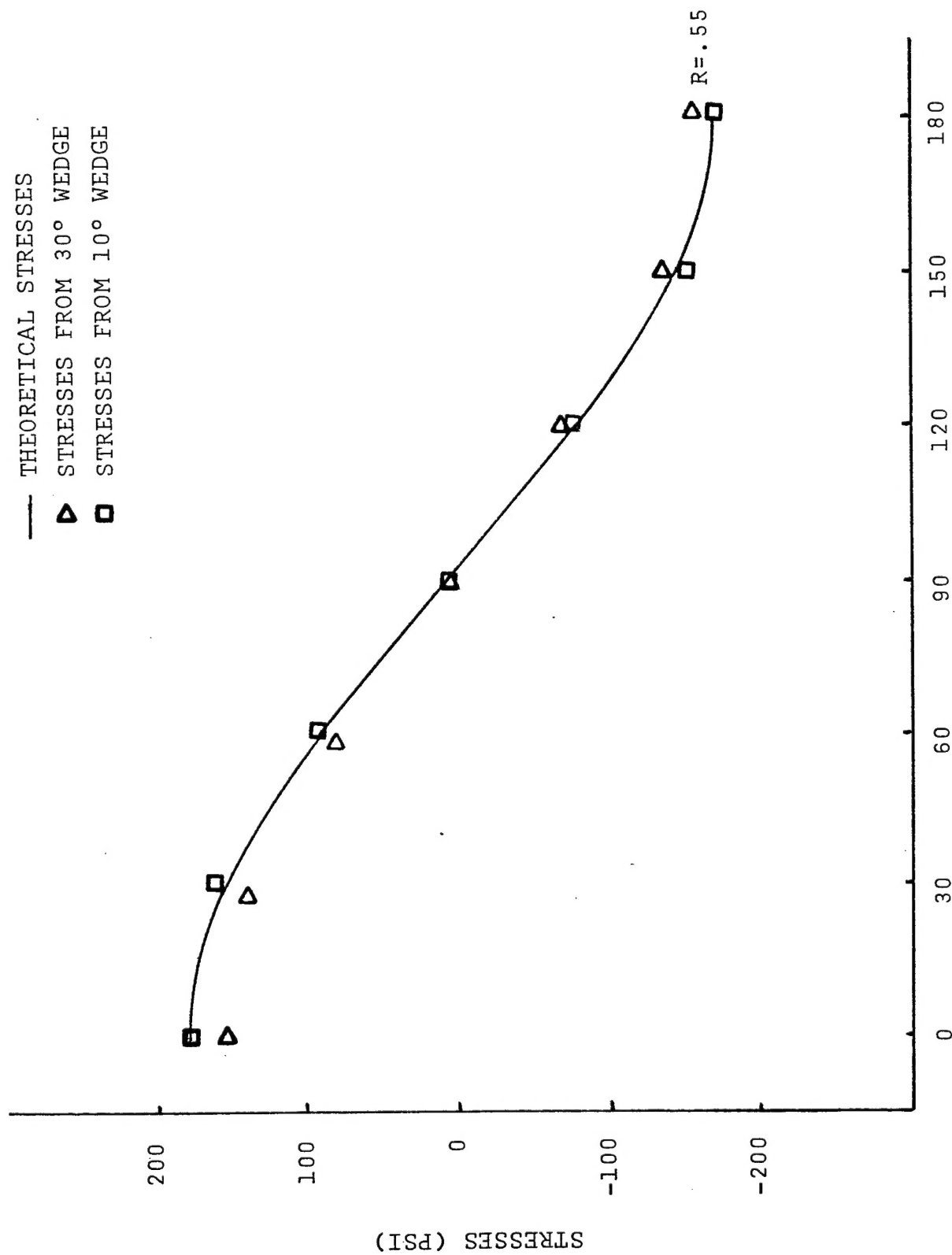


Figure 16. Hoop Stress as a Function of Angle for a Radius of .55 Inches in the Asymmetrically Heated Ring

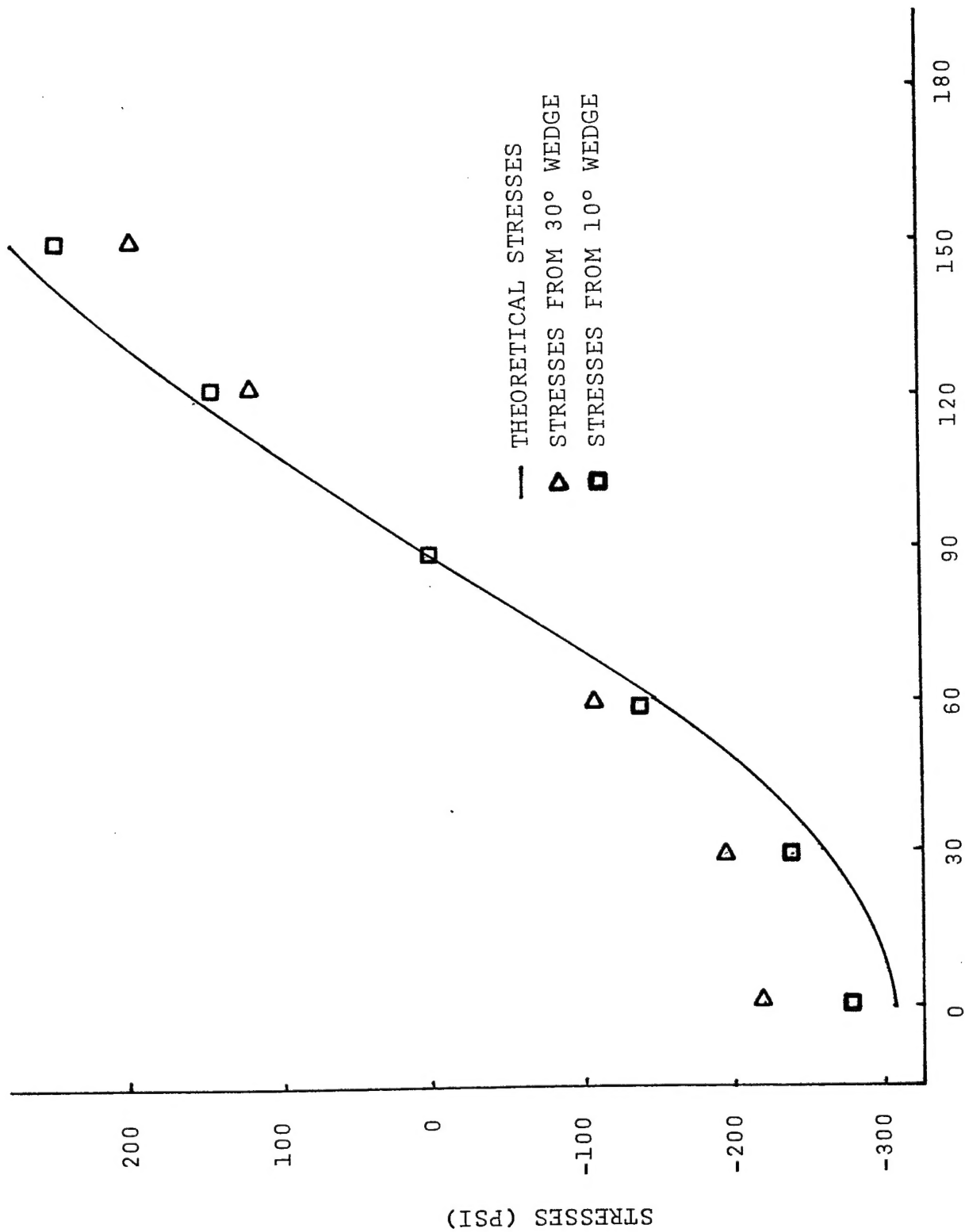


Figure 17. Hoop Stress as a Function of Angle for a Radius of .95 Inches in the Asymmetrically Heated Ring

required that the CTRAPAX elements be rectangular, while the cyclic symmetry option did not have this limitation. The following is a comparison of the running time on level 16.0 NASTRAN with 32 elements in each model.

	<u>CYCLIC SYMMETRY TECHNIQUE</u>		<u>AXISYMMETRIC TECHNIQUE</u>
	(30° Wedge)	(10° Wedge)	(15° Increments)
CM(octal)	165,000	170,000	250,000
CP(sec)	445	1,200	2,681
IO(sec)	333	869	307

These results indicate that the cyclic symmetry option in NASTRAN is better suited to the solution of a general axisymmetric problem under asymmetric loading than the axisymmetric technique.

#### REFERENCES

1. Wang, C. T., "Applied Elasticity," McGraw-Hill Book Co., Inc., 1953.
2. Maddux, G. E., "Thermo-Structural Analysis Manual," Report No. WADD-TR-60-517, Vol. 1, August 1962.
3. Negaard, G. R. and Paul, D. B., "The Structural Analysis of a Silicon Nitride Radome Subjected to Aerodynamic Heating," Report No. AFFDL-TM-73-135-FBE, December 1973.
4. Anon, "The NASTRAN User's Manual," Level 16.0, NASA SP-222(04), 1979.